Nanoscale

Accepted Manuscript

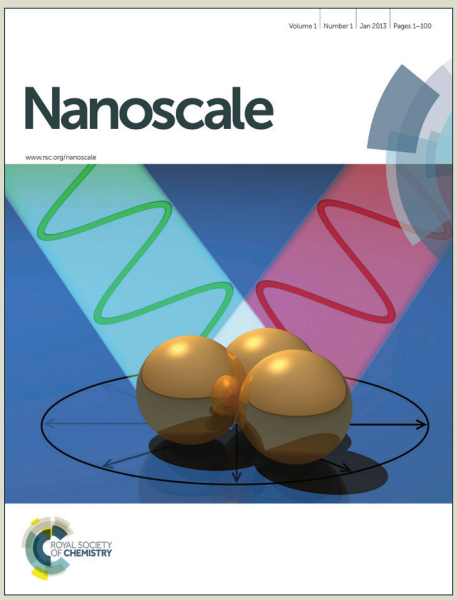

ROYAL SOCIETY OF CHEMISTRY

www.rsc.org/nanoscale

Rague-Like FeP Nanocrystal Assembly on Carbon Cloth: An Exceptionally Efficient and Stable Cathode for Hydrogen Evolution

Xiulin Yang, Ang-Yu Lu, Yihan Zhu, Shixiong Min, Mohamed Nejib Hedhili, Yu Han, Kuo-Wei Huang and Lain-Jong Li*

[#]*Physical Sciences and Engineering, King Abdullah University of Science and Technology, Thuwal, 23955-6900, Kingdom of Saudi Arabia.*

[*]To whom correspondence should be addressed: (L. J. Li) lance.li@kaust.edu.sa

KEYWORDS: Hydrogen evolution reaction; Iron phosphide; Electrolysis; Catalysis

BRIEFS: High surface area FeP nanosheets on carbon cloth prepared by gas phase phosphidation of electroplated FeOOH exhibits exceptionally high catalytic efficiency and stability for hydrogen generation.

ABSTRACT

There is a strong demand to replace expensive Pt catalysts with cheap metal sulfides or phosphides for hydrogen generation in water electrolysis. The earth-abundant Fe can be electroplated on carbon cloth (CC) to form high surface area ragues-like FeOOH assembly. Subsequent gas phase phosphidation converts the FeOOH to FeP or FeP_2 and the morphology of the crystal assembly is controlled by the phosphidation temperature. The FeP prepared at 250 ^{o}C presents lower crystallinity and those prepared at higher temperatures 400 ^{o}C and 500 ^{o}C possess higher crystallinity but lower surface area. The phosphidation at 300 ^{o}C produces nanocrystalline FeP and preserves the high-surface area morphology; thus it exhibits the highest HER efficiency in 0.5 M H_2SO_4; i.e. the required overpotential to reach 10 and 20 mA/cm^2 is 34 and 43 mV respectively. These values are lowest among the reported non-precious metal phosphides on CC. The Tafel slope for the FeP prepared at 300 ^{o}C is around 29.2 mV/dec comparable to that of Pt/CC,

indicating that the hydrogen evolution for our best FeP is limited by Tafel reaction (same as Pt). Importantly, the FeP/CC catalyst exhibits much better stability in a wide range working current density (up to 1 V/cm^2), suggesting that it is a promising replacement of Pt for HER.

Table of Content

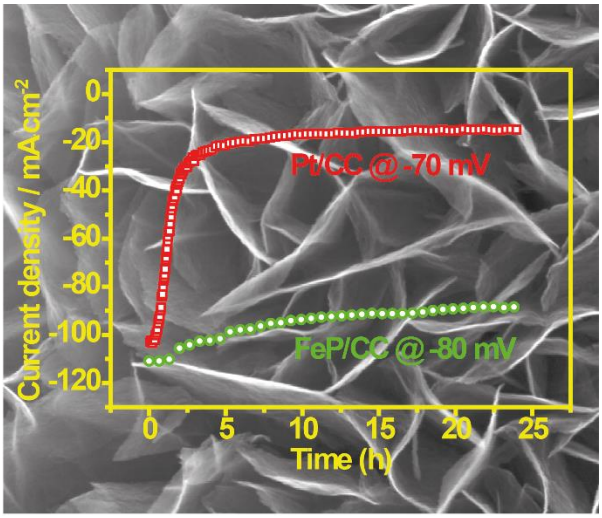

Hydrogen is a clean energy carrier for replacing petroleum fuels to relieve issues associated with global warming. Water splitting by electrolyzer is one of the most promising and efficient methods to produce hydrogen on demand.[1-3] Among many different cathode materials, pure Platinum (110) exhibits the highest efficiency in the hydrogen evolution reaction (HER).[4, 5] However, the high cost and limited source of Pt retards its large scale applications. Many research efforts have been focused on several more economical materials which may be suitable replacements for Pt cathodes, such as molybdenum sulfide,[6-12] Mo_2C,[13-18] MoB,[19] MoN[20, 21] and metal phosphides. It is recently noted that the transition metal phosphides of Mo, W, Fe, Co and Ni have shown significant advances in HER efficiency.[22-39] The content for Fe, Ni, Co, Mo and Pt in the Earth's crust is estimated to be 50000, 80, 20, 1.5 and 0.003 ppm respectively.[40] It is apparent that Fe, the fourth most common element in the Earth's crust, is a very attractive material for large-scale catalysis. Hence, the possibility of using iron phosphide as an HER catalyst in an acidic solution has been extensively studied.[29-34] FeP_2 was obtained by the pyrolysis of ferrocene and red phosphorous.[28] Nanoporous FeP nanosheets were prepared by ion-exchange synthesis using $Fe_{18}S_{25}$ and

trioctyl-phosphine as sources.[34] Alternatively, FeP nanoparticles were synthesized by gas phase phosphidation of Fe_3O_4 nanoparticles at 350 ^oC.[33] These reports have demonstrated a Tafel slope ranging from 59 to 67 mV/dec. Very recently, dense FeP nanowire array has been achieved by chemical phosphidation of the hydrothermally grown FeOOH nano array,[30] where the Tafel slope of the system has been further lowered to 38 mV/dec. Various Tafel slopes explored from these results indicate that the synthetic method significantly affect the HER mechanisms for the FeP catalysts. In addition to the active FeP materials, the selection of acid-resistant conducting substrates for HER are limited to novel metals, Ti, and carbon materials. Carbon cloth (CC) is cheap, highly conductive and flexible. It has become one of the popular substrates used for electrocatalysis. In this contribution, we perform the direct electroplating of Fe on carbon cloth and convert it to FeOOH or Fe_2O_3 at various oxidation temperatures. Controlled gas phase phosphidation reveals that nanocrystalline FeP obtained with the phosphidation temperature at 300 ^oC exhibits better HER performance than the highly crystalline FeP and FeP_2 phosphidated at a higher temperature 400 or 500 ^oC. For the best FeP catalyst, the required overpotential to reach 10 and 20 mA/cm^2 (η_{10} and η_{20}) is 34 and 43 mV respectively. These values are lowest among the reported non-precious metal phosphides on CC. Although the values are slightly higher than the 29 and 36 mV for the Pt coated CC (Pt/CC), the FeP nanocrystal based HER catalysts exhibit much better stability than Pt/CC in a wide range of working current density (up to 1 A/cm^2 in our test), demonstrating that FeP/CC catayst is an attractive Pt alternative for the practically used water electrolysis systems.

RESULTS AND DISCUSSIONS

Formation of FeOOH coating on Carbon Cloth: Fig. 1a shows the scanning electron microscopy (SEM) images for the surafces of the carbon cloth used in this study, where the surface of the fibers in CC is smooth and its diameter is around 9 μm. The electroplating of Fe on carbon cloth is performed in a 0.1 M $FeSO_4$ solution and the subsequent oxidation in air forms a layer of uniform coating on the fiberous structure of CC as shown in the SEM images of Fig. 1b. The electroplating time is optimized at 20 min as described in Methods. The magnified SEM image reveals that the

layer of coating is composed of many randomly oriented micron-sized sheets perpendicularly grown on the fiber surfaces. These sheets assemble to form ragues-like morphologies, which are beneficial for catalytic reaction owing to its high surface area. Fig. 1c displays the X-ray diffraction (XRD) pattern for these electrochemically deposited layer. The peaks can be well indexed to the polycrystalline α- and γ-FeOOH, indicating that the deposited layer is a mixture of α- and γ-FeOOH crystallites.

Vapor Phase Phosphidation: The vapor phase phosphidation is carried on in a two-zone chemical vapor deposition (CVD) furnace, where the NaH_2PO_2 is dissociated at 300 ^oC to form PH_3 gases.[41] The produced PH_3 vapors are brought to the FeOOH on CC at the downstream site which can be set at a desired reaction temperature such as 250, 300, 400, and 500 ^oC. Fig. 2a schematically illustrates the set-up for the gas phase phosphidation. We observe that the FeOOH structures start to be phosphidated with the vapor phase reaction at the temperature $\geq$250 ^oC. Note that the phosphidation of FeOOH does not occur when the temprature is lower than 200 ^oC. The XRD results in Fig. 2b show that the orthorombic FeP crystals form after phosphidation at 400 ^oC and some FeP_2 also appears after 500 ^oC phosphidation. All peaks are well indexed to orthorombic FeP or FeP_2.[28] When the phosphidation temperature is at 300 ^oC or lower, the diffraction peaks are relatively broader, suggesting that the resulted crystals are small in size or contain some amorphous phases. The SEM photos in inset of Fig. 2b show the surface morphology of the sample phosphidated at each temperature, where the rugae-like morphology from the deposited FeOOH still sustains after phosphodiation at 250 or 300 ^oC. A higher temperature such as 400 and 500 ^oC wrecks the rugae-like structures and the micro-size sheets become aggregated. The transmission electron microscopy (TEM) images in Fig. 3 demonstrate that the small sample flakes peeled off from the FeP/CC prepared at 300 ^oC consists of rich FeP nanocrystallites with some amorphous structures, where the crystallites are only few nanometer in lateral size. Electron diffraction (ED) tells that these crystallites are randomly oriented. It is noted that the FeP/CC preapred at 250 ^oC consists of similar nanocrystalline structures (see TEM images in Fig. S1) but the nanocrystal density is lower than that prepared at 300 ^oC.

It is noted that the gas phase phosphidation of FeOOH is more efficient than that of iron oxides. We have separately converted the electroplated FeOOH/CC to Fe_2O_3/CC by heating the sample to 400 ^oC in air for 4 h. The subsequent phosphidation at 300 ^oC cannot efficiently convert Fe_2O_3 to FeP. The XRD result in Fig. S2 demonstrates that Fe_2O_3 structure still remains and only part of the Fe_2O_3 is converted to Fe_3O_4 and FeP. The HER performance for the obtained catalyst (via phosphidation) is rather poor, where the required overpotential η_{10} and η_{20} are 46 and 59 mV respectively (Fig. S3). . Hence, the control of the chemical structure of the electroplated Fe is critical for achieving better phosphidation. We will focus our discussions on the catalysts prepared from FeOOH only.

HER Characteristics for FeP/CC Catalysts: Fig. 4a shows the polarization curves for the catalysts prepared at different phosphidation temperatures, where the loading amount for each FeP sample is determined as 4.9 mg on 1 cm^2 of CC. Since the same carbon cloth is used as the substrate to load different catalysts including Pt for comparison, we use the the geometrical area of CC to normalize the measured HER current in all cases. Note that the potential (V) used here is already after internal resistance (IR) drop compensation. Meanwhile, it is worthy that the RHE calibration is crucially important to ensure that the overpotential is correct (see methods for details). We observe that the HER current decreases with the increasing phosphidation temperature from 300 to 500 ^oC, indicating that the highly crystalline FeP or FeP_2 is not necessarily better for HER. The Pt/CC we use is prepared by electrochemical deposition of 5 mg Pt from the K_2PtCl_6 solution. As expected, the Pt/CC exhibits excellent HER efficiency (overpotential η_{10} = 29 mV and η_{20} = 36 mV *vs.* RHE). The corresponding overpotential η_{10} and η_{20} for the catalyst phosphidated at 300 ^oC are 34 mV and 43 mV. Although the values are slightly higher than those of Pt/CC, the values are lowest among the reported non-precious metal phosphides on CC as shown in Table 1. Fig. 4b shows that the extracted Tafel slope for the four FeP/CC catalysts prepared at 250 ^oC, 300 ^oC, 400 ^oC and 500 ^oC. The Tafel slope for the FeP/CC prepared at 250 ^oC is 30.4 mV/dec, close to the 29.2 mV/dec for the FeP/CC prepared at 300 ^oC. This suggests that the HER catalyzed by nanocrystalline orthorombic FeP is the

same as Pt, dominated by the Tafel recombination step (Catalyst-H + Catalyst-H → H_2 + 2 Catalyst).[6] The Tafel slope for the FeP/CC prepared at 400 ^oC (highly crystalline orthorombic FeP) is 39.7 mV/dec, indicating that the HER proceeds with a Volmer-Heyrovsky mechanism and the rate-determing step is the Heyrovsky reaction (Catalyst-H + H^+ + e^- → H_2 + Catalyst).[15] The Tafel slope further increases to 51.4 mV/dec for the FeP/CC preapred at 500 ^oC (a mixture of FeP and FeP_2). It is noted that low Tafel slope is desirable for the practical high working current density HER since a lower applied voltage to drive the water electrolysis is beneficial. The HER characteristics for the four FeP catalysts are also summarized in Table 1.

We perform the scanning rate measurement for these samples to extract their capacitance of the double layer at the solid-liquid interface (see Fig. S4 for details). Fig. 4c summarizes the obtained double-layer capacitance for each sample, from which we conclude that a higher HER efficiency (or lower overpotential η_{10} and η_{20}) well correlates to a higher double-layer capacitance. This implies that the HER efficiency variation is related to the difference in capacitance. Note that the double-layer capacitance is a non-Faradic capacitance which is rather nice gauge for the interfacial area between the surface of the electrode and an electrolyte. In other words, the effective surface area of the catalysts based on highly crystalline FeP or FeP_2 is lower than the samples phosphidated at 300 ^oC. The lower capacitance for the FeP prepared at higher tempratures are also in line with the SEM observation as shown in Fig. 2b, where the ragued-like morphologes are not well sustained. It is likely that the high surface area from rugae-like morphology significantly contributes to the high performance HER.

Chemical Bonding Structures of FeP/CC prepared at 300 ^oC: X-ray photoelectron spectroscopy (XPS) was employed to characterize the chemical bonding structures of our FeP/CC sample, in which Fe, O, P, C elements are detected as shown in the survey scan in Fig. S5a. Fig. S5b and S5c display the high resolution XPS spectra of the Fe 2p and P 2p core levels, where the characteristic peaks for Fe $2p_{3/2}$, Fe $2p_{1/2}$, P $2p_{3/2}$ and P $2p_{1/2}$ are observed at 707.2 eV, 720.2 eV, 129.3 eV and 130.2 eV respectively. The peaks at 707.2 eV and 129.3 eV are assigned to the binding energies for

Fe and P in FeP nanocrystals,[30] and the peaks at 720.2 eV and 133.3 eV can be attributed to the oxidized Fe and P species which could be partly due to the oxidation in air.[29] The XPS results confirm the presence of FeP and some oxidized FeP and Fe. In addition, some residual elementary Fe which remains un-oxidized or un-phosphidated is also found in the structure but it is considered as an inert impurity since Fe metal is much less active in HER.

Estimation of Active Site Number: The underpotential deposition (UPD) of copper has been used to extract the density of active sites for Pt[42] and WS_2,[43] where they observe that the coverage and surface density of the copper is the same as that for adsorbed hydrogen on the HER catalyst surface. Hence, the surface activity of HER catalysts can be determined by measuring the charges exchanged during the stripping of the copper deposited at the under potential regions. The optimal condition for measuring active sites of our FeP is in a solution with 0.5 M H_2SO_4 and 20 mM $CuSO_4$. Fig. 5a displays the current–voltage scan for FeP formed at 300 ^oC, where the regions for UPD, overpotential deposition (OPD) and their stripping are clearly observed. Fig. 5b shows the charges required to strip the Cu (Q_{Cu2+}) deposited at different underpotentials. We find that the Q_{Cu2+} for the UPD at 0.22 and 0.24 V has already involved OPD of Cu (see supporting Fig. S6 for details). There is no OPD involved when the copper is deposited at the voltage 0.26 V or above. Hence, the flat area in the middle potential is the regime where UPD occurs but OPD is still not yet possible. The Q_{Cu2+} plateau in between UPD 0.26 V and 0.32 V allows us to extract the active sites number. The Q_{Cu2+} at UPD 0.26 V is 0.1328 C, meaning that 6.68×10^{-7} mol of Cu (0.1328/96500/2) has been deposited. The active site density is estimated as 1.36×10^{-7} mol/mg = 8.2×10^{16} sites/mg, where the density is apparently higher than those for the FeP catalysts formed at 400 ^oC and 500 ^oC (shown in supporting Fig. S7). The active site density results also agree well with double layer capacitance results in Figure 4c. Note that the active site density for the Pt/CC estimated using the same method is 2.7×10^{16} sites/mg, which is about 1/3 of our FeP/CC catalyst (see supporting Fig. S8 for the estimation of active site density for Pt/CC).

HER Stability of the FeP/CC: In addition to the high HER efficiency, the catalyst also presents excellent stability in acidic solutions. Fig. 6a displays the time dependent measurement for FeP/CC and Pt/CC at a low working current density (*ca.* 100 mA/cm^2). It is observed that the decay of HER current for FeP/CC is 20% after 24 h but the decaly is 85% for Pt/CC likely due to the well-known aggregation of Pt and/or poisoning by carbon monoxide.[44] Actually the surface of CC is relatively smooth as shown in Figure 1(a). Thus, the Pt tends to aggregate during the electrocatalytic reaction. Another commonly known reason is the poisoning of Pt surface by carbon monoxide and other impurities. By contrast, the active FeP is embedded in a three dimensional structure which can effectively inhibit the aggregation. Hence, FeP/CC is more stable than Pt/CC. Fig. 6b presents the HER stability at a high working current density (*ca.* 1A/cm^2), where FeP/CC does not show obvious current decay after HER for 24 h but Pt/CC exhibits 13% of decay after HER. The better HER stability at high working current densities is likely due to that the quick hydrogen bubble generation inhibits the CO poisoning more efficiently. Based on the experimental results, it is concluded that FeP/CC is relatively more stable than Pt/CC in an acidic solution and hence it is an excellent replacement for Pt.

CONCLUSIONS

In summary, iron phosphide was synthesized by vapor phase phosphidation of the FeOOH obtained by electroplating. The ragued-like morphology formed during the electroplating provides a large surface area. The subsequent phosphidation at 300 ^{o}C converts the FeOOH to nanocrystalline FeP while maintaining the ragued morphology. The Tafel slop reaches 29.2 mV/dec, close to that of Pt/CC. The low Tafel slop, the high HER performance (η_{10} = 34 mV/dec and η_{20} = 43 mV/dec) and excellent stability of FeP/CC suggest that it is a promising replacement of Pt for HER. The morphology and the crystal structures of FeP seem to strongly affect the HER characteristics. It is anticipated that more research efforts in this area may bring these cheap catalysts to practical applications in the near future.

METHODS

Materials: All chemical reagents used in this experiment were of analytical grade. Ferrous sulfate heptahydrate ($FeSO_4·7H_2O$), sodium hypophosphite (NaH_2PO_2), sodium hydroxide (NaOH), nitric acid (HNO_3), sulfuric acid (H_2SO_4) and ethanol were used as received without further purification. The water used throughout all experiments was purified through a Millipore system.

Synthesis of FeOOH on carbon cloth: The carbon cloth (CC, 1 cm × 2.5 cm) was repeatedly washed using deionized water and ethanol to remove impurities and maintain the wettability of the CC. The CC was then quickly inserted into 0.1 M $FeSO_4$ (immersed geometric area 1 cm^2) as a working electrode. The 0.1 M $FeSO_4$ was prepared by dissolving 1.112 g (4 mmol) $FeSO_4·7H_2O$ in 40 mL Milli-Q water at room temperature (~23 ^oC). Pt foil and Ag/AgCl (in 3 M KCl solution) electrode were used as the counter and reference electrodes, respectively. Constant current electroplating was conducted at -10 $mA·cm^{-2}$ typically for 20 min in a PGSTAT 302N Autolab workstation. Freshly prepared samples were then exposed to air for overnight. It is noted that the HER performance of Fe/CC increases with the FeOOH electroplating time and 20 min is found as the optimized electroplating time. Further increase in time degrades the HER performance (see Fig. S9 for details). In this report, we use 20 min as the electroplating for all samples.

Preparation of FeP on carbon cloth: In a typical experiment, the NaH_2PO_2 in a porcelain boat was put in the upstream side and FeOOH/CC in another boat was placed at the downstream side in a furnace. First, the acquired samples were heated to different temperatures with a heating speed of 2 °C/min in an Ar flowing atmosphere (60 sccm). Subsequently, the NaH_2PO_2 was quickly heated to the temperature of 260 ^oC in 10 min, and then slowly raised to 300 ^oC with a heating speed of 1 ^oC/min to transport the generated PH_3 to the substrate. After the reaction, the samples were immersed into 0.5 M H_2SO_4 and Milli-Q water for 20 min respectively to dissolve the impurities. After dried in vacuum oven, the loading of FeP on CC was determined to be 4.9 $mg·cm^{-2}$ using a high precision weighing balance.

Electrochemical Measurements: The electrochemical measurements were performed in a PGSTAT 302N Autolab Potentiostat/Galvanostat (Metrohm) at room temperature. Graphite rod and Ag/AgCl (in 3 M KCl solution) electrode were used as counter and reference electrodes, respectively. The reference electrode was calibrated for the reversible hydrogen potential in the electrolyte solution purged with Ar for 30 min prior to measurements. In a 0.5 M H_2SO_4 solution, E (RHE) = E (Ag/AgCl) + 0.207 + 0.059pH. The pH value for our solution is 0.35 and hence the equation becomes E (RHE) = E (Ag/AgCl) + 0.228. The validity of the Nernst equation used in our study has been verified by our separate RHE calibration. The calibration was done in a high purity hydrogen saturated electrolyte with a Pt wire as the working electrode (see Supporting Fig. S10 for details), where the measurement (0.225 V offset) agrees well with the value 0.228 V mentioned above. In the manuscript, we take a more preservative offset value 0.225 for calibration. The electrocatalytic activity of FeP towards HER was examined by obtaining polarization curves using linear sweep voltammetry (LSV) at a scan rate of 0.5 $mV \cdot s^{-1}$ in 0.5 M H_2SO_4 solution. The time dependent current density of the FeP was tested in 0.5 M H_2SO_4 at an overpotential of 80 mV (*vs.* RHE). All data have been corrected for a small ohmic drop (~1.7 Ω) based on impedance spectroscopy.

Characterization: The morphologies of the catalysts were determined by filed-emission scanning electron microscope (FESEM, FEI Quanta 600) and transmission electron microscopy (FEI Titan ST, operated at 300 KV). The crystalline structure of the samples was analyzed by X-ray diffraction (XRD, Bruker D8 Discover diffractometer, using Cu Kα radiation, λ = 1.540598 Å). XPS studies were carried out in a Kratos Axis Ultra DLD spectrometer equipped with a monochromatic Al Kα x-ray source (hν = 1486.6 eV) under a vacuum of 1×10^{-9} mbar. The spectra were collected at fixed analyzer pass energies of 160 eV and 20 eV, respectively. Binding energies were referenced to the C 1s peak (set at 284.4 eV) of the sp^2 hybridized (C=C) carbon from the sample.

ACKNOWLEDGMENTS:

This research was supported by KAUST.

Supporting Information Available: Fig. S1-S10 are included. See DOI: 10.1039/x0xx00000x.

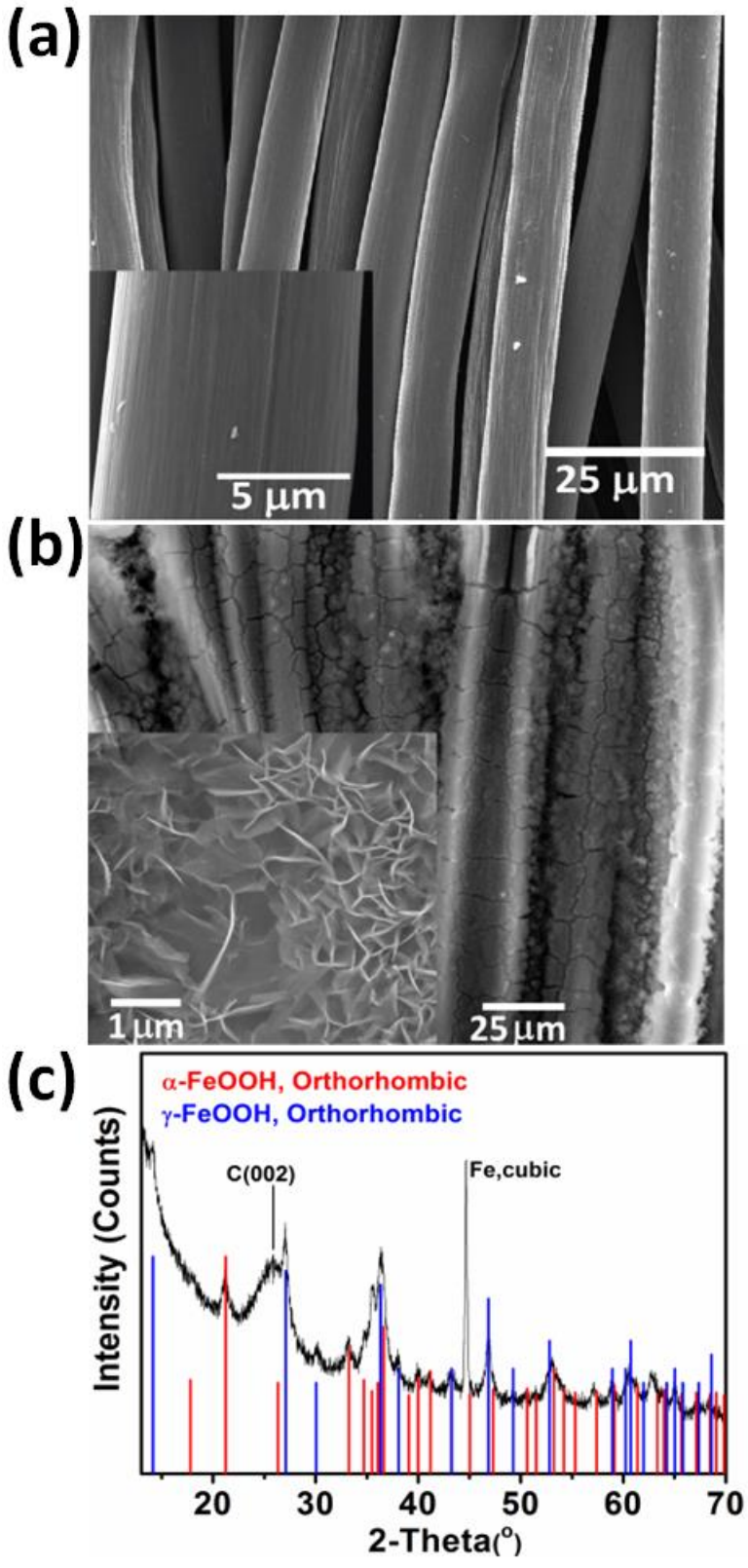

Fig. 1 (a) SEM image for the pristine carbon cloth. (b) SEM image for the FeOOH formed after oxidation of the electroplated Fe on carbon cloth. (b) XRD pattern shows the presence of α- and γ-phase FeOOH as indexed.

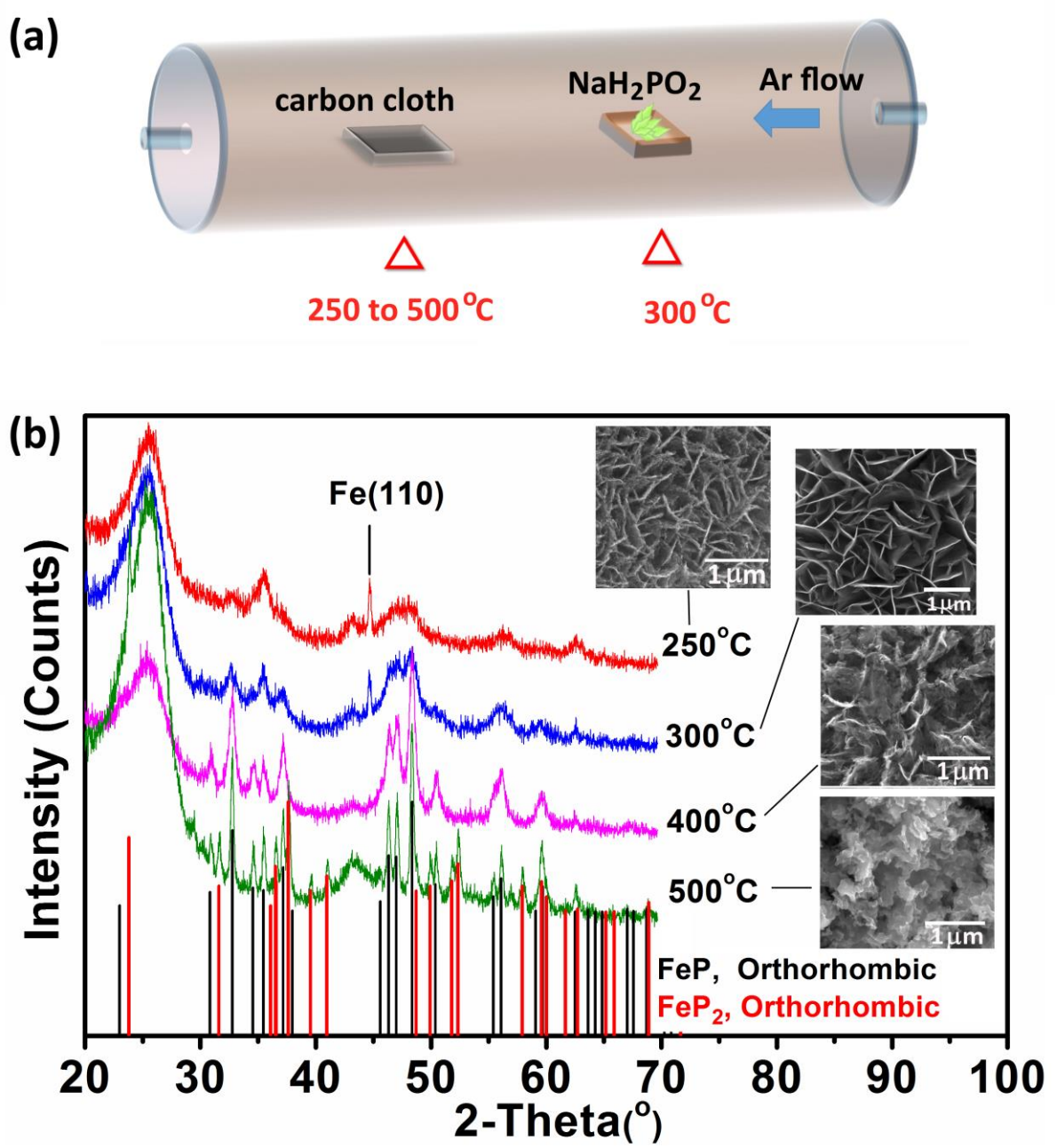

Fig. 2 (a) Schematic illustration for the phosphidation process. (b) XRD patterns and SEM images for the FeOOH/cabon cloth samples after phosphidation at varied temperatures.

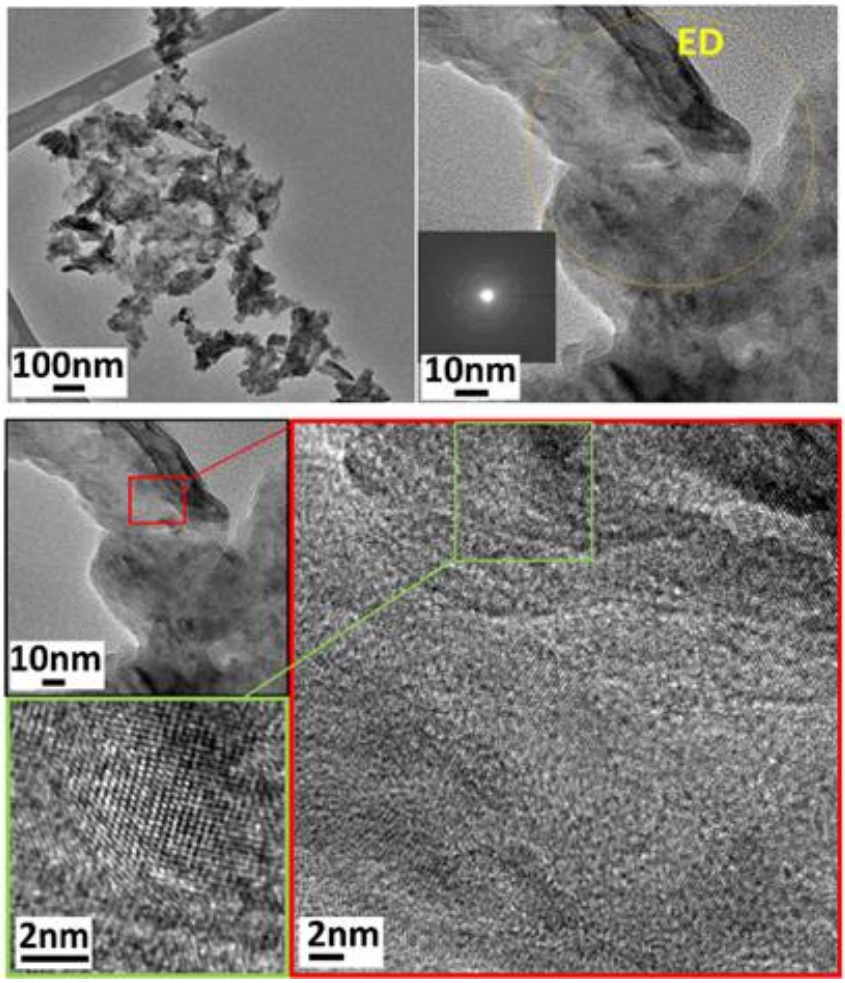

Fig. 3 TEM images for the FeP catalyst phosphidated at 300 ^{o}C.

.

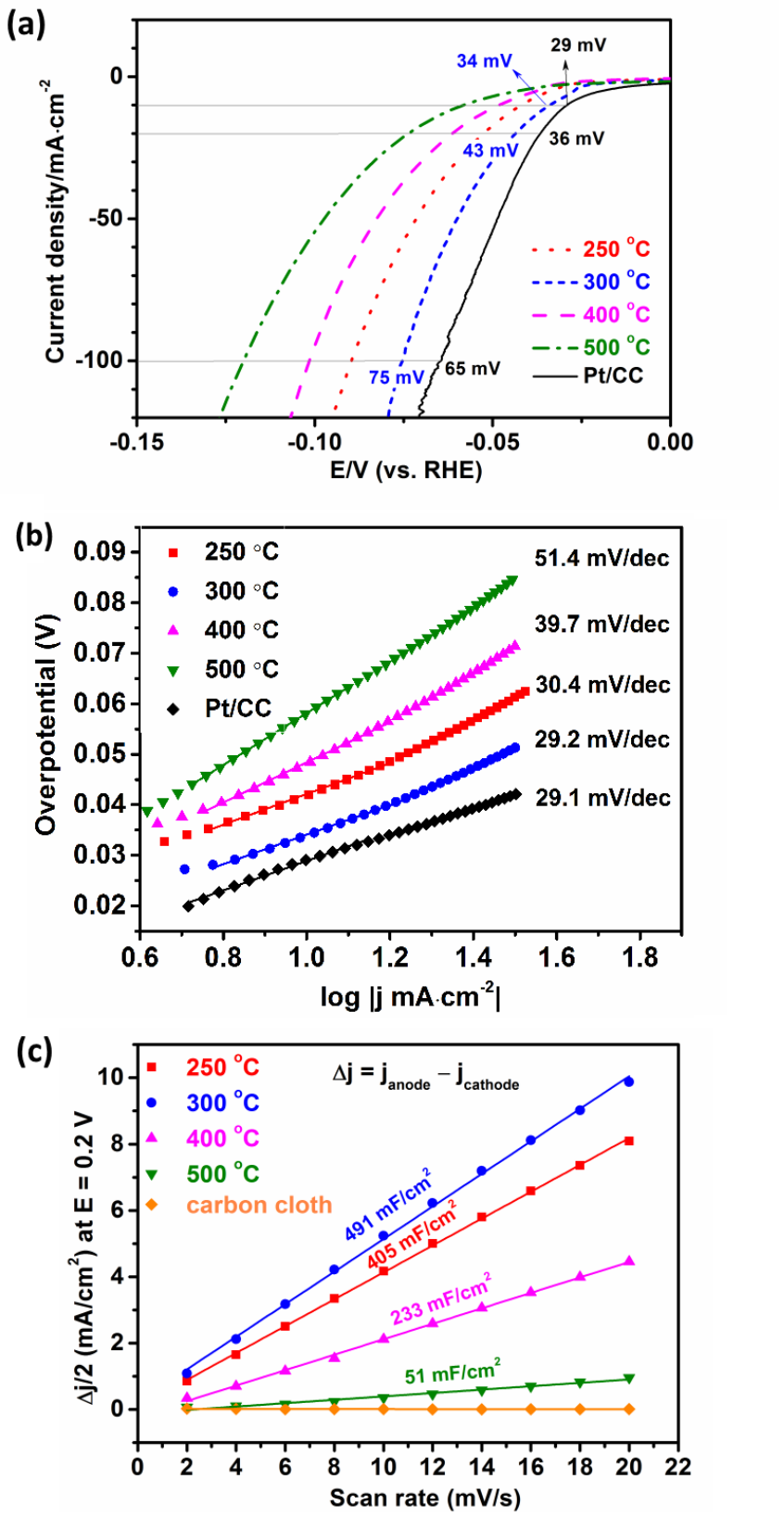

Fig. 4 (a) The polarization curves for the catalysts prepared at different phosphidation temperatures, where the current is normalized by the geometrical area of carbon cloth and the potential is after internal resisitance correction. (b) Tafel slopes extracted from the polarization curves in (a). (c) double-layer capacitance for the corresponding catalysts prepared at different phosphidation temperatures.

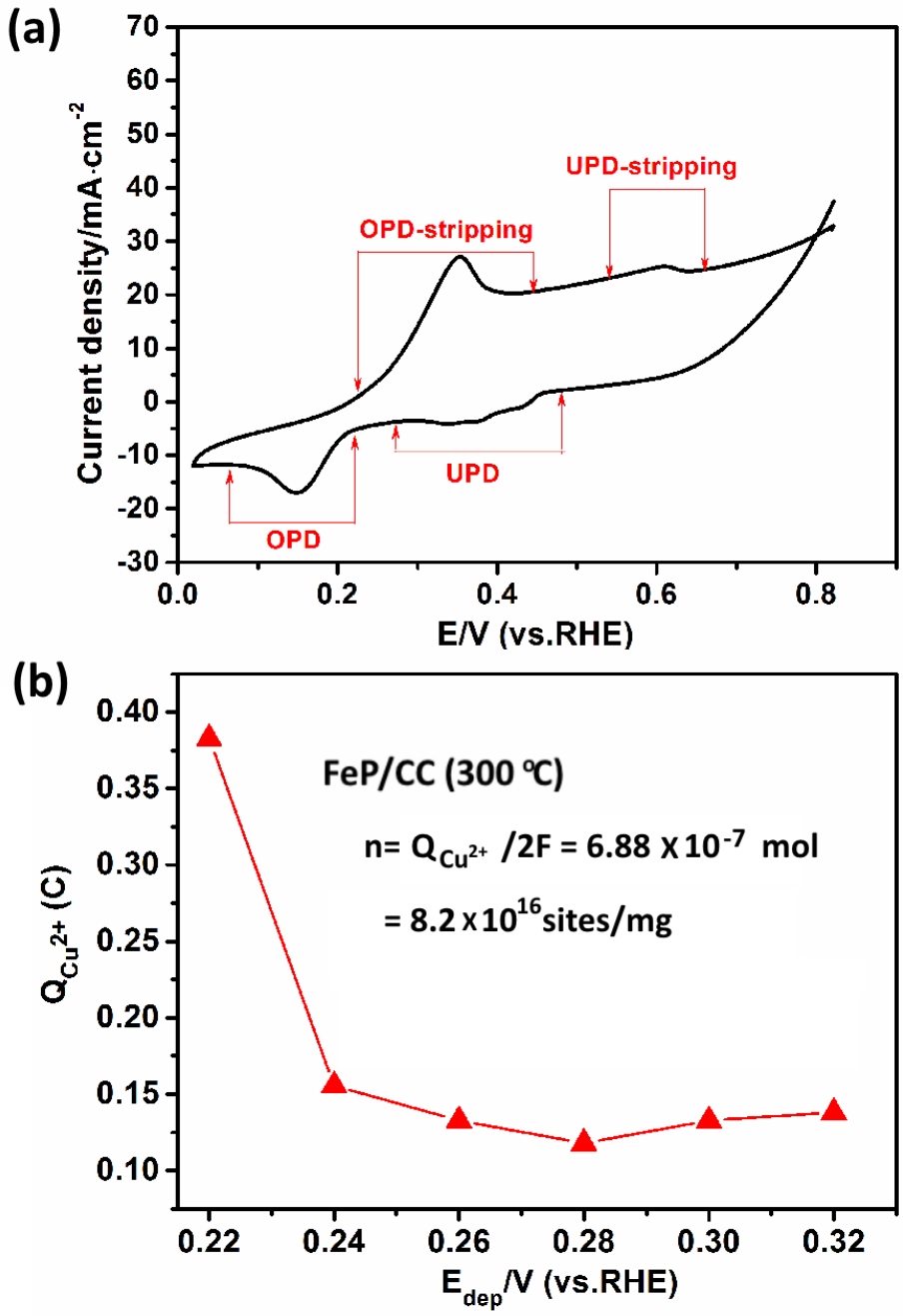

Fig. 5 (a) The current–voltage scan for the FeP catalyst formed at 300 ^{o}C (Scan procedure: from positive to negative and then positive voltages). The electrochemical processes UPD, OPD, OPD-stripping and UPD-stripping are observed in sequence. (b) The charges required to strip the Cu deposited at different under potentials.

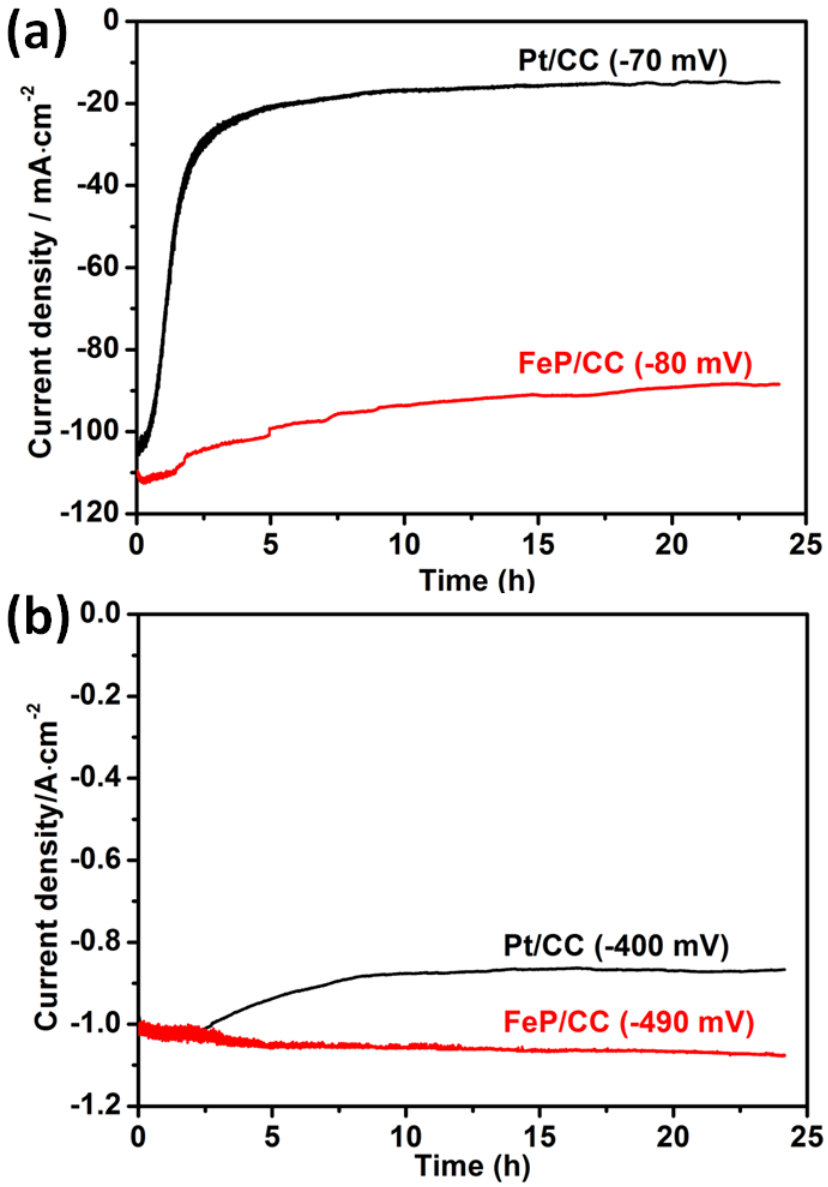

Fig. 6 Time-dependent HER performance for the FeP phosphidated at 300 ^{o}C at a (a) low working current density and (b) high working current density. The voltage values indicated are after IR-correction.

Table 1. Summary of HER performance in 0.5M H_2SO_4 for recently published non-precious metal phosphide catalysts loaded on carbon cloth. The values report in the Table were taken directly from literature. It is noted that particular attention should be paid when comparing the overpotential (η_{10} and η_{20}) and exchange current density in different reports since various the potential calibration methods for reference electrodes were used.

Catalyst	Catalyst loading (mg/cm^2)	η_{10} (mV)	η_{20} (mV)	Tafel slope (mV/dec)	J_0 (mA/cm^2)
Pt (this work)	5.0	29	36	29.1	1.02
FeP (300°C) (this work)	4.9	34	43	29.2	0.68
FeP (250°C) (this work)	4.9	42	53	30.4	0.41
FeP (400°C) (this work)	4.9	49	61	39.7	0.60
FeP (500°C) (this work)	4.9	58	74	51.4	0.74
FeP[29]	4.2	39	54	32	0.59
MoS_2[45]	0.19	160	180	50	0.0092
WS_2[45]	1.5				
WP[46]	2.0	-	130	69	0.29
CoP[37]	0.92	67	100	51	0.288
NiP_2[47]	4.3	75	99	51	0.26
CoP[48]	4.0	48		70	
$CoSe_2$[49]	2.5~3.0	137	150	40	0.0049

REFERENCES

1. Z. Zeng, C. Tan, X. Huang, S. Mao and H. Zhang, *Energy Environ. Sci.*, 2014, **7**, 797-803.
2. J. Chen, X.-J. Wu, L. Yin, B. Li, X. Hong, Z. Fan, B. Chen, C. Xue and H. Zhang, *Angew. Chem. Int. Ed.*, 2015, **54**, 1210-1214.
3. J. Yang, D. Voiry, S. J. Ahn, D. Kang, A. Y. Kim, M. Chhowalla and H. S. Shin, *Angew. Chem. Int. Ed.*, 2013, **52**, 13751-13754.
4. W. Sheng, Z. Zhuang, M. Gao, J. Zheng, J. G. Chen and Y. Yan, *Nat. Commun.*, 2015, **6**, 5848.
5. R. Subbaraman, D. Tripkovic, D. Strmcnik, K.-C. Chang, M. Uchimura, A. P. Paulikas, V. Stamenkovic and N. M. Markovic, *Science*, 2011, **334**, 1256-1260.
6. Y. Li, H. Wang, L. Xie, Y. Liang, G. Hong and H. Dai, *J. Am. Chem. Soc.*, 2011, **133**, 7296-7299.
7. M. A. Lukowski, A. S. Daniel, F. Meng, A. Forticaux, L. Li and S. Jin, *J. Am. Chem. Soc.*, 2013, **135**, 10274-10277.

8. Y. W. Tan, P. Liu, L. Y. Chen, W. T. Cong, Y. Ito, J. H. Han, X. W. Guo, Z. Tang, T. Fujita, A. Hirata and M. W. Chen, *Adv. Mater.*, 2014, **26**, 8023-8028.
9. Y.-H. Chang, C.-T. Lin, T.-Y. Chen, C.-L. Hsu, Y.-H. Lee, W. Zhang, K.-H. Wei and L.-J. Li, *Adv. Mater.*, 2013, **25**, 756-760.
10. Y.-H. Chang, F.-Y. Wu, T.-Y. Chen, C.-L. Hsu, C.-H. Chen, F. Wiryo, K.-H. Wei, C.-Y. Chiang and L.-J. Li, *Small*, 2014, **10**, 895-900.
11. A. J. Smith, Y.-H. Chang, K. Raidongia, T.-Y. Chen, L.-J. Li and J. Huang, *Adv. Energy Mater.*, 2014, **4**, 1400398.
12. T.-Y. Chen, Y.-H. Chang, C.-L. Hsu, K.-H. Wei, C.-Y. Chiang and L.-J. Li, *Int. J. Hydrogen Energy*, 2013, **38**, 12302-12309.
13. K. Zhang, Y. Zhao, S. Zhang, H. Yu, Y. Chen, P. Gao and C. Zhu, *J. Mater. Chem. A*, 2014, **2**, 18715-18719.
14. K. Xiong, L. Li, l. zhang, W. Ding, l. peng, Y. Wang, S. Chen, S. Tan and Z. Wei, *J. Mater. Chem. A*, 2015, **3**, 1863-1867.
15. L. Liao, S. Wang, J. Xiao, X. Bian, Y. Zhang, M. D. Scanlon, X. Hu, Y. Tang, B. Liu and H. H. Girault, *Energy Environ. Sci.*, 2014, **7**, 387-392.
16. W. F. Chen, C. H. Wang, K. Sasaki, N. Marinkovic, W. Xu, J. T. Muckerman, Y. Zhu and R. R. Adzic, *Energy Environ. Sci.*, 2013, **6**, 943-951.
17. C. Wan, Y. N. Regmi and B. M. Leonard, *Angew. Chem. Int. Ed.*, 2014, **53**, 6407-6410.
18. N. S. Alhajri, D. H. Anjum and K. Takanabe, *J. Mater. Chem. A*, 2014, **2**, 10548-10556.
19. H. Vrubel and X. Hu, *Angew. Chem. Int. Ed.*, 2012, **124**, 12875-12878.
20. W.-F. Chen, K. Sasaki, C. Ma, A. I. Frenkel, N. Marinkovic, J. T. Muckerman, Y. Zhu and R. R. Adzic, *Angew. Chem. Int. Ed.*, 2012, **51**, 6131-6135.
21. B. Cao, G. M. Veith, J. C. Neuefeind, R. R. Adzic and P. G. Khalifah, *J. Am. Chem. Soc.*, 2013, **135**, 19186-19192.
22. M. S. Faber and S. Jin, *Energy Environ. Sci.*, 2014, **7**, 3519-3542.
23. D. Kong, J. J. Cha, H. Wang, H. R. Lee and Y. Cui, *Energy Environ. Sci.*, 2013, **6**, 3553-3558.
24. H. S. Shin and J. Yang, *J. Mater. Chem. A*, 2013, **2**, 5979-5985.
25. G. Sun, J. Liu, X. Zhang, X. Wang, H. Li, Y. Yu, W. Huang, H. Zhang and P. Chen, *Angew. Chem. Int. Ed.*, 2014, **53**, 12576-12580.
26. Z. Huang, C. Lv, Z. Chen, Z. Chen, F. Tian and C. Zhang, *Nano Energy*, 2015, **12**, 666-674.
27. Z. Huang, Z. Chen, Z. Chen, C. Lv, H. Meng and C. Zhang, *ACS Nano*, 2014, **8**, 8121-8129.
28. J. Jiang, C. Wang, J. Zhang, W. Wang, X. Zhou, B. Pan, K. Tang, J. Zuo and Q. Yang, *J. Mater. Chem. A*, 2015, **3**, 499-503.
29. J. Tian, Q. Liu, Y. Liang, Z. Xing, A. M. Asiri and X. Sun, *ACS Appl. Mater. Interfaces*, 2014, **6**, 20579-20584.
30. P. Jiang, Q. Liu, Y. Liang, J. Tian, A. M. Asiri and X. Sun, *Angew. Chem. Int. Ed.*, 2014, **53**, 12855-12859.
31. J. F. Callejas, J. M. McEnaney, C. G. Read, J. C. Crompton, A. J. Biacchi, E. J. Popczun, T. R. Gordon, N. S. Lewis and R. E. Schaak, *ACS Nano*, 2014, **8**, 11101-11107.
32. R. Liu, S. Gu, H. Du, A. M. Asiri and C. Li, *J. Mater. Chem. A*, 2014, **2**, 17263-17267.
33. Z. Zhang, B. Lu, J. Hao, W. Yang and J. Tang, *Chem. Commun.*, 2014, **50**, 11554-11557.

34. Y. Xu, R. Wu, J. Zhang, Y. Shi and B. Zhang, *Chem. Commun.*, 2013, **49**, 6656-6658.
35. Q. Liu, J. Tian, W. Cui, P. Jiang, N. Cheng, A. M. Asiri and X. Sun, *Angew. Chem. Int. Ed.*, 2014, **53**, 6710-6714.
36. E. J. Popczun, C. G. Read, C. W. Roske, N. S. Lewis and R. E. Schaak, *Angew. Chem. Int. Ed.*, 2014, **53**, 5427-5430.
37. J. Tian, Q. Liu, A. M. Asiri and X. Sun, *J. Am. Chem. Soc.*, 2014, **136**, 7587-7590.
38. L. Feng, H. Vrubel, M. Bensimon and X. Hu, *Phys. Chem. Chem. Phys.*, 2014, **16**, 5917-5921.
39. E. J. Popczun, J. R. McKone, C. G. Read, A. J. Biacchi, A. M. Wiltrout, N. S. Lewis and R. E. Schaak, *J. Am. Chem. Soc.*, 2013, **135**, 9267-9270.
40. K. Barbalace, *EnvironmentalChemistry*, 1995-2015.
41. N. Shamim and K. Sharma Virender, eds., *Sustainable Nanotechnology and the Environment: Advances and Achievements*, American Chemical Society, 2013.
42. C. L. Green and A. Kucernak, *J. Phys. Chem. B*, 2002, **106**, 1036-1047.
43. D. Voiry, H. Yamaguchi, J. Li, R. Silva, D. C. B. Alves, T. Fujita, M. Chen, T. Asefa, V. B. Shenoy, G. Eda and M. Chhowalla, *Nat. Mater.*, 2013, **12**, 850-855.
44. D. Merki and X. Hu, *Energy Environ. Sci.*, 2011, **4**, 3878-3888.
45. Y. Yan, B. Y. Xia, N. Li, Z. J. Xu, A. C. Fisher and X. Wang, *J. Mater. Chem. A*, 2015, **3**, 131-135.
46. Z. Pu, Q. Liu, A. M. Asiri and X. Sun, *ACS Appl. Mater. Interfaces*, 2014, **6**, 21874-21879.
47. P. Jiang, Q. Liu and X. Sun, *Nanoscale*, 2014, **6**, 13440-13445.
48. Q. Li, Z. Xing, A. M. Asiri, P. Jiang and X. Sun, *Int. J. Hydrogen Energy*, 2014, **39**, 16806-16811.
49. D. Kong, H. Wang, Z. Lu and Y. Cui, *J. Am. Chem. Soc.*, 2014, **136**, 4897-4900.